CSIC
CONSEJO SUPERIOR DE INVESTIGACIONES CIENTÍFICAS

EUMETSAT
OSI SAF
OCEAN AND SEA ICE

Royal Netherlands
Meteorological Institute
Ministry of Infrastructure and the Environment

Ocean and Sea Ice SAF

Scientific Report

SAF/OSI/CDOP3/KNMI/SCI/RP/344

Enhanced Quality Control with the NSCAT-5 Geophysical Model Function

Marcos Portabella

Wenming Lin

Ad Stoffelen

A. Verhoef

Z. Wang

Version 1.1

17 April 2019

DOCUMENTATION CHANGE RECORD

Reference: **OSI_AVS_17_04**

Issue / Revision :	Date :	Change :	Description :
Version 1.0	2018-12-05	Marcos Portabella	Draft version
Version 1.1	2019-03-04	Ad Stoffelen	Revision
Version 1.1	2019-03-07	Marcos Portabella	Revision
Version 1.1	2019-03-09	Ad Stoffelen	Revision
Version 1.1	2019-04-17	Marcos Portabella	Report title change

Summary

Recent developments on the wind geophysical model function (GMF) of Ku-band scatterometers include a sea surface temperature (SST) dependent term. It has been found that the SST effects on the radar backscatter are wind speed dependent and more pronounced in vertical polarization (VV) than in horizontal polarisation (HH) at higher incidence angles, and are mainly relevant at Ku radar wavelengths rather than at C-band. The new Ku-band GMF, NSCAT-5, was initially based on a physical model and RapidScat radar backscatter measurements, which are only available at two incidence angles, i.e., 48.8^0 and 55.2^0, for HH and VV beams, respectively.

A more recent CDOP-2 AS study (OSI_AVS_17_01) confirms only small differences when verifying the NSCAT-5 GMF at similar incidence angles, using data from the recently-launched Indian SCATSat-1, which operates at 49.1^0 (HH) and 57.9^0 (VV) incidence angle. In order to further consolidate the NSCAT-5 GMF, the current study looks for quality control (QC) dependencies. It is found that indeed, the developed GMF is not particularly sensitive to different QC thresholds. Finally, an improved QC method, based on the successful experience with previous Ku-band rotating pencil-beam scatterometers, is developed for SCATSat-1 data.

Contents

1 Introduction

Users of the European Organisation for the Exploitation of Meteorological Satellites (EUMETSAT) Ocean and Sea Ice (OSI) Satellite Application Facility (SAF) products noted geographically-dependent biases, violating a fundamental paradigm in NWP data assimilation, called Best Linear Unbiased Estimate (BLUE)[1]. Collocated Ku- and C-band data helped identify sea surface temperature (SST) as the main contributing factor to these local biases [1], but also led to the introduction of stress-equivalent reference wind, accounting for air mass density, which also geographically varies [2]. The resulting SST dependency of the Ku-band Geophysical Model Function (GMF), which is different for VV and HH polarization, affects in turn the compromise of the backscatter measurements in the different views during wind retrieval and therefore potentially affects the local minimum distance between the backscatter measurements and the associated GMF-simulated backscatter values at the retrieved wind speed and direction. A normalized residual backscatter distance, called MLE, is successfully used for Quality Control (QC) of Ku-band scatterometer winds [3]. Therefore, it is relevant to investigate the changes in the distribution of this distance, called MLE, and its effects on QC, which is the objective of this study.

Beyond SST, the remaining ancillary dependencies are expected to be yet smaller and well below the 1% level. The ocean normalized radar cross section (NRCS, σ^0) or backscatter measured by satellite scatterometer systems is representative of the sea surface roughness at the scale of gravity-capillary waves, which are dominated by mean sea-surface winds, but also modulated by some secondary geophysical effects, such as SST, increased wind variability [4] or (mainly for Ku-band systems) the presence of rain [3]. The radar backscatter is also a function of atmospheric and ocean mass density [2], the viewing geometry (incidence and azimuth angles), radar properties (polarization and frequency), and electromagnetic sea water properties, which are assumed constant here.

Since the fundamental understanding of physical processes of the ocean surface backscatter is insufficient at the moment, empirical approaches are used to derive GMFs in practice. These GMFs give the radar backscatter as a function of several physical parameters, fitted to a large number of observations. Improving GMFs is a continuous effort and new versions are being developed over time, e.g., CMOD5 [5], C-2015 [6], and CMOD7 [7] for C-band, and for Ku-band SASS GMF [8], NSCAT-1 [9], NSCAT-4 [10], OSCAT GMF [11], Ku-2011 [12] and NSCAT-5 [13]. GMF improvement is generally based on the analysis of wind and inversion residuals as a function of the GMF parameters, where the residuals may be obtained from the wind retrieval process or from comparison to reference stress-equivalent wind data sets [2]. Naturally, wind and inversion residuals may also depend on parameters that are not yet part of the GMF, such as for example wind variability, waves, rain, or SST.

In [1] and [13], the variations of backscatter due to SST changes, depending on scatterometer radar frequency, polarization, and incidence angle, are investigated on the basis of a physics-based radar backscatter model and a dataset of collocated C-band (Advanced scatterometer or ASCAT) and Ku-band (RapidScat) scatterometer measurements. The study shows that the SST effects are substantial at Ku-band, but rather negligible for C-band backscatter measurements. Moreover, the SST effects are wind speed dependent and more pronounced in VV polarization and at higher incidence angles,

[1] Wind Bias Correction Guide, v1.3 (NWPSAF-KN-UD-007)
High resolution data assimilation guide, v1.2 (NWPSAF-KN-UD-008)

the latter according to the physics-based backscatter model. Other effects, such as Sea Surface Salinity (mainly corresponding to ocean mass density variations), e.m. water properties and waves, on scatterometer winds are limited (generally well within 1%). As a result, a new Ku-band GMF, NSCAT-5, which includes a SST-dependent term, has been developed.

While NSCAT-5 actually models the sensitivity of the Ku-band radar backscatter to sea surface wind for a wide range of incidence angles from 22° to 59°, the GMF was only verified for one incidence angle per polarization (48.8° for HH and 55.2° for VV) using RapidScat data. In a recent study [14], a similar approach to [13] is used to analyse the sensitivity of SCATSat-1 radar backscatter to SST under different wind conditions. The results reveal only small differences when NSCAT-5 is verified with SCATSat-1, which operates at slightly different incidence angles (49.1° for HH and 57.9° for VV) than RapidScat.

In order to further consolidate the NSCAT-5 GMF, this study focuses on potential GMF dependencies to different quality control (QC) thresholds. Moreover, a more effective QC, based on two quality-sensitive parameters, the inversion residual [15] and an image processing technique, i.e., the so-called singularity analysis [16], is developed for SCATSat-1 data. Section 2 describes the datasets used. In Section 3, the GMF sensitivities to different thresholds of the current operational QC are analysed. In Section 4, the new SCATSat-1 QC is developed. Finally, the conclusions and the outlook are presented in section 5.

2 Data

Ten months (October 2016 - July 2017) of collocated ASCAT-A (onboard Metop-A satellite) 25-km Level 2 (L2) winds and SCATSat-1 scatterometer stress-equivalent winds are analyzed. Both data sets are in Binary Universal Format Representation (BUFR), and are provided by the EUMETSAT OSI SAF. The scatterometer data sets already include collocated European Centre for Medium-range Weather Forecasts (ECMWF) model stress-equivalent winds, which are estimated by interpolating three ECMWF 3-hourly forecast winds on a 62.5-km grid both spatially and temporally to the scatterometer data acquisition location and time, respectively. The SCATSat-1 winds are processed with the Level 2A (L2A) version 1.1.3 (v1.1.3) backscatter (σ^0) "egg" data, using the NWP SAF Pencil-beam scatterometer Wind Processor (PenWP) with the NSCAT-4 GMF [17] (section 3) and NSCAT-5 [18] (section 4). The latter consists of NSCAT-4 with direction and speed corrections, and the consolidated SST σ^0 corrections tailored for ScatSat-1 incidence angles. In order to further improve the SCATSat-1 QC, a second data set of SCATSat-1 data collocated with GMI rain data (obtained from the Remote Sensing Systems web site www.remss.com/missions/gmi) over the same period is also used in section 4.

A σ^0-dependent correction for σ^0 values above -19 dB is used to correct for increasing wind speed biases above ~15 m/s due to the non-linearity in the backscatter values. Then a constant correction of 1.08 dB /0.35 dB for the HH/VV beams is applied to bring the average signal levels to the model values (using ECMWF winds as input) and to minimise wind speed biases[2].

The ASCAT winds are reprocessed using the ASCAT Wind Data Processor (AWDP) with the CMOD7 GMF [6], which is based on a combination of CMOD5.N and C2013 (particularly for low

[2] ScatSat-1 Product User Manual

winds) [19][20][21], and has been constrained to provide a uniform wind speed probability density function (PDF) over the entire swaths of ASCAT and the scatterometer onboard the European Remote Sensing Satellite (ERS).

The collocation criteria are less than 30 minutes distance in time and 25 km distance in space between SCATSat-1 and ASCAT measurements. Note that all SCATSat-1 winds across the inner swath are used in analysis. The total amount of collocations is about 28 million, with 26.6 million quality-control (QC) accepted data. Figure 1(a) illustrates the geographical distribution of the collocated ASCAT-SCATSat data, while Figure 1(b) shows the two-dimensional histogram of the collocations as a function of temporal (*y*-axis) and spatial (*x*-axis) distances.

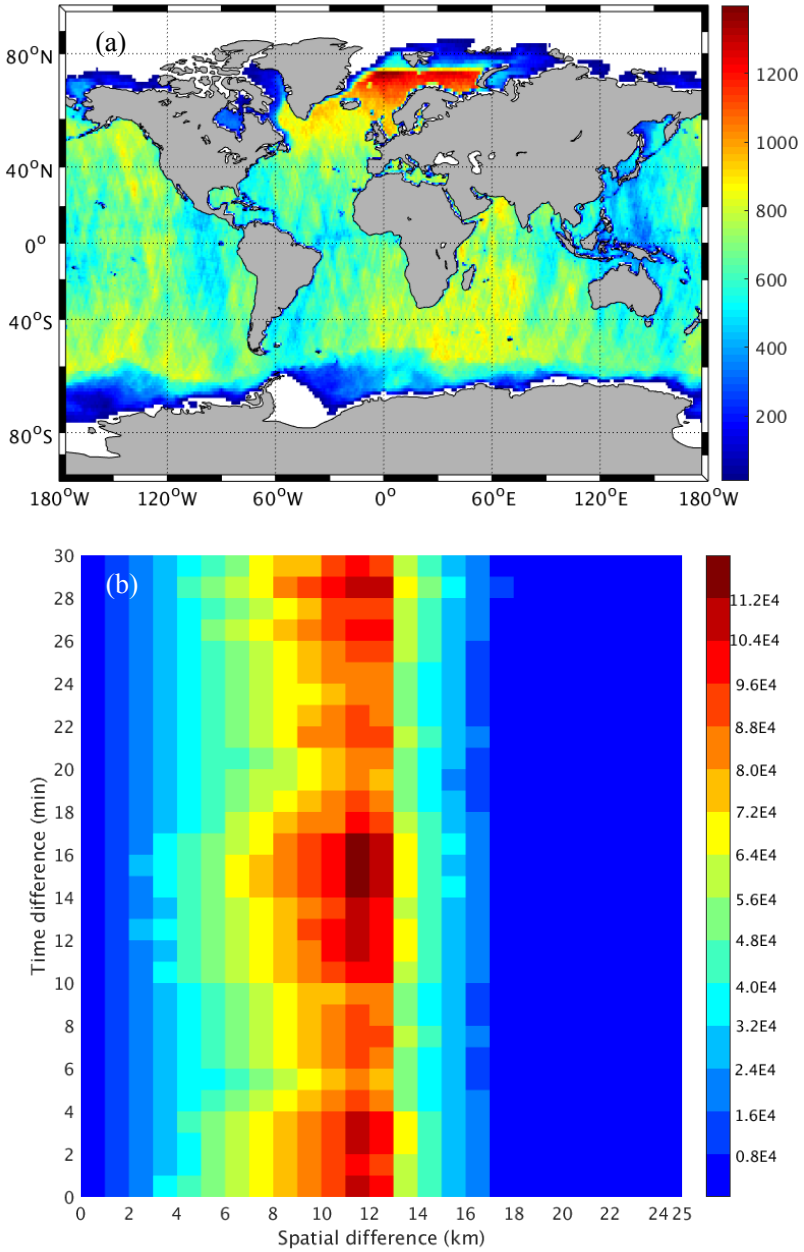

Fig. 1 (a) The geographical distribution of the collocated ASCAT-SCATSat data, latitude and longitude bins of 1°; (b) Two-dimensional histogram of the collocations as a function of temporal and spatial distances, bins of 1 minute and 1 km respectively.

3 GMF dependencies on QC

In this section, similar plots to those in [14] are shown, but for different QC strategies. In particular, two different QCs are used, one less conservative and another more conservative than the one used in [14]. In particular, the QC used in [14] uses the following criteria: only collocations with a MLE value below 5 (for both ASCAT and SCATSat-1) and a wind speed difference between ASCAT and SCATSat-1 below 5 m/s are used. This QC (hereafter referred to as the reference or REF-QC) leads to 86.9% of QC-passed data.

In this study, the operational ASCAT and SCATSat-1 QCs, which are based on instrument-specific MLE thresholds, are also analyzed. The operational QC (KNMI-QC) leads to 94.6% of QC-passed data, i.e., a less conservative QC than REF-QC. In addition, a more conservative QC (i.e., the rigorous or RIGO-QC), by setting a fraction of 0.3 to the SCATSat-1 operational MLE threshold, is also used, which leads to 75.6% of QC-passed data.

3.1 Analysis of wind speed differences

In practice, the SST dependency of the Ku-band backscatter is derived from the analysis of binned observations and simulations. Following [13], ASCAT winds are considered to be independent of SST, and are therefore used as reference.

Figure 2 shows the mean wind speed differences between the three available data sources (i.e., ASCAT, SCATSat-1, and ECMWF) as a function of the averaged wind speed. Note that all combinations show systematic differences as a function of wind speed. Note that the difference between ASCAT and SCATSat-1 winds does not significantly depend on QC (i.e., the red-solid and red-dashed lines are very close to each other).

Following [14], a speed-dependent bias correction is applied to ASCAT winds in order to match the C- and Ku-band speed distributions. The correction factor is formulated as

$$\Delta V_{SA} = \overline{V_S - V_A}(v) \tag{1}$$

where ΔV_{SA} is the mean speed difference between SCATSat-1 (V_S) and ASCAT (V_A) winds as a function of the averaged speed v. The corrected ASCAT wind speed is then

$$V_A' = V_A + \Delta V_{SA}(V_A) \tag{2}$$

with the remaining speed difference defined as

$$\Delta V_{SA}' = V_S - V_A' \tag{3}$$

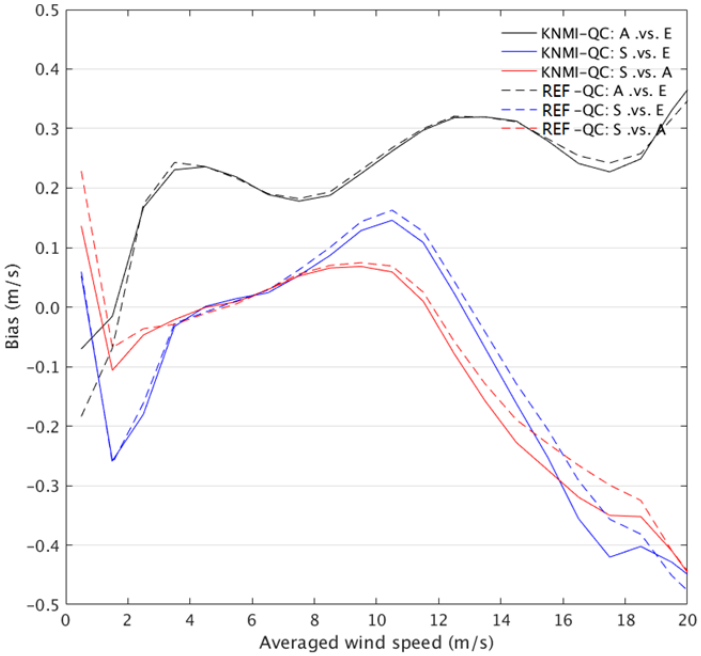

Fig. 2 Mean wind speed difference between ASCAT and ECMWF (black curve), SCATSat-1 and ECMWF (blue curve), and SCATSat-1 and ASCAT (red curve), as a function of the averaged wind speed of each pair of wind sources, with a binning of 1 m/s. The solid (dashed) lines correspond to KNMI-QC (REF-QC) data. Note that ECMWF winds are real 10-m winds and about 0.2 m/s higher [24][3], while ASCAT and SCATSat-1 are 10-m stress-equivalent winds.

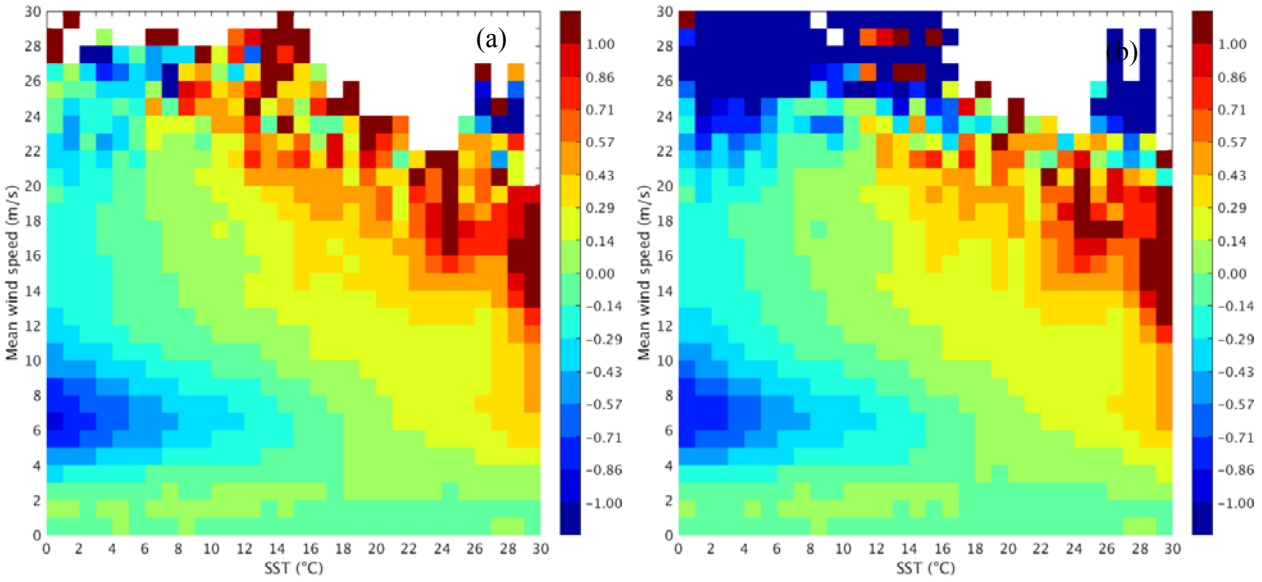

Fig. 3 Mean wind speed difference (m/s) between SCATSat-1 and ASCAT-corrected winds ($\Delta V'_{SA}$) as a function of averaged wind speed and SST, for the REF-QC (a) and the KNMI-QC (b) datasets. The wind speed and SST are binned every 1 m/s and 1°C, respectively.

Figure 3 shows $\Delta V'_{SA}$ as a function of average wind speed and SST, for both REF-QC (a) and KNMI-QC (b) datasets. Note that $\Delta V'_{SA}$ does not show any significant dependency on QC, except for winds higher than 25 m/s. The reason for this difference is that REF-QC is rejecting a much

larger amount of high winds than KNMI-QC.

3.2 SST dependence analysis

The observed SCATSat-1 backscatter values at wind speed $V = \frac{1}{2}(V_A' + V_S)$ and SST T are denoted as $\sigma^0_{p,obs}(V,T)$. The simulated backscatters using NSCAT-4 and SCATScat observation geometry are denoted as $\sigma^0_{p,sim}(V,T) = \sigma^0_{p,sim}(V_A', T_{GMF})$. T_{GMF} is determined by the mean SST of the sea surface measurements which were used to derive NSCAT-4 [8]. T_{GMF} is actually a function of wind speed (not shown). Figure 4 shows the mean observed (left for REF-QC, and right for KNMI-QC) and simulated backscatter values as a function of SST for the wind speed range 5.5 m/s<V<6 m/s. As in [14], the simulated backscatter values show no significant dependence on SST, indicating that the SCATScat sampling is similar to that of the NASA Scatterometer (NSCAT), which was used to derive the NSCAT-4 GMF, while the real backscatter measurements (solid lines) show a clear SST dependence, more pronounced in VV (red) than in HH (black). Again, the curves do not show much sensitivity to QC. Note though that for the KNMI-QC dataset the observed curves are more irregular (noisier) than for the REF-QC dataset. This is not due to lack of data since the KNMI-QC actually contains about 8% more data than the REF-QC (see Fig. 5). In contrast, this irregularity may be caused by the fact that the KNMI-QC dataset contains more high wind variability conditions and/or presence of rain than the REF-QC dataset, which indeed impact the observed σ^0 sensitivities. A stricter QC appears thus beneficial for the derivation of geophysical dependencies.

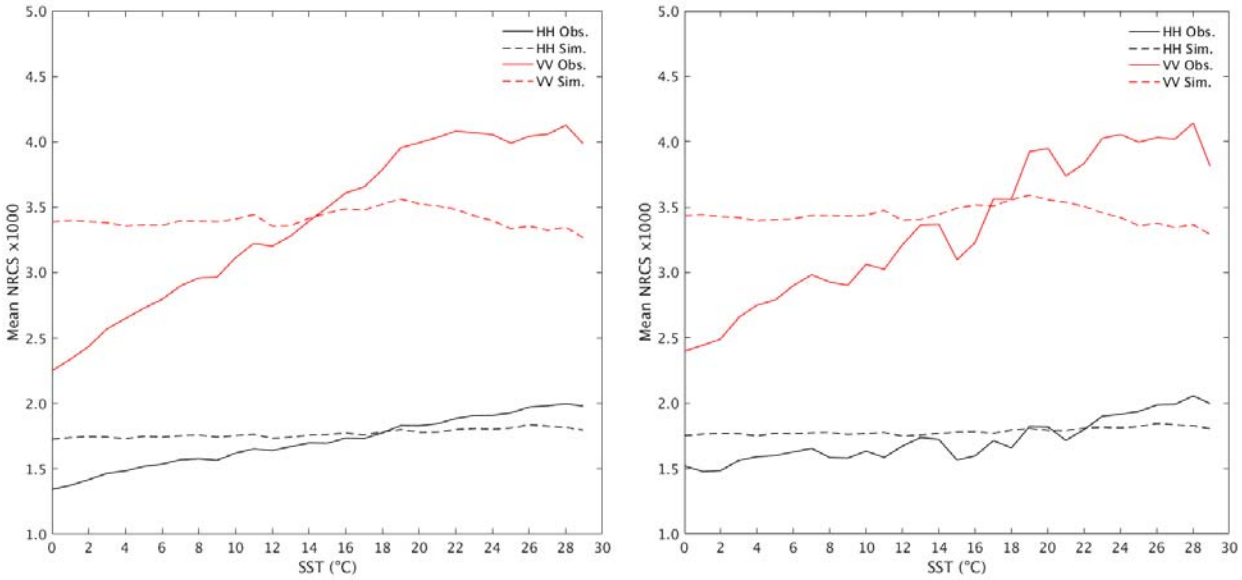

Fig. 4 The mean observed (solid) and simulated (dashed) NRCS (value times 1000) as a function of SST for wind speed of 5.5 m/s<V<6 m/s. The black curves are for HH polarisation and the red curves for VV polarisation. The observed σ^0s correspond to REF-QC (left) and KNMI-QC (right) datasets.

It is clear that higher SST generally corresponds to more water vapour in the atmosphere and thus heavier rain. Heavy rain clearly causes the backscatter from clouds to saturate and results in typical-

ly 15 m/s wind speeds. One thus may expect a high rejection ratio near 15 m/s, particularly at high SST. On the other hand, [25] notes enhanced global rain and snow frequency at the higher ocean latitudes, i.e., at lower SST. Fig.5 shows the rejection ratio as a function of SST for different SCATSat-1 wind speed intervals, and for both the REF-QC (left) and the KNMI-QC (right) datasets. As already mentioned, REF-QC leads to a larger number of rejections than the KNMI-QC. Note also that the rejection ratio is rather uniform across SST and wind speeds for the KNMI-QC, whereas it shows a more pronounced SST dependence as well as a very distinct pattern for low-medium winds and high winds for the REF-QC. Seemingly, many low and moderate winds at low SST are rejected, where small precipitation amounts may suffice to add backscatter variability (cf. the noise reduction in Figure 4a). Given the expected more dense and deep rain clouds at high SST, indeed, REF-QC also rejects more data at high speeds and high SST than KNMI-QC, probably benefitting a rain-free GMF fitting of SST sensitivity.

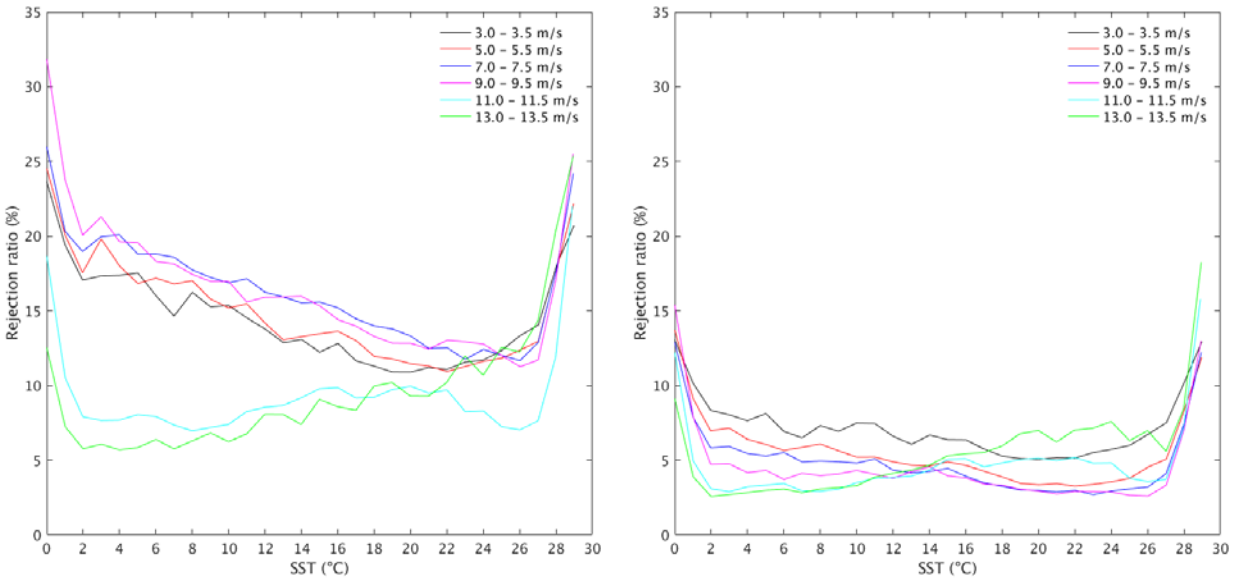

Fig.5 Rejection ratio as a function of SST for different SCATSat-1 wind speed intervals (see colour legend), and for both the REF-QC (left) and the KNMI-QC (right) datasets.

As expressed in [13] and [14], the improved NSCAT-5 model (*abbr.* N_5) that includes SST dependency can be easily derived from NSCAT-4 (*abbr.* N_4) by applying the following correction:

$$GMF_{N5} = f_p(V,T) \times GMF_{N4} \tag{4}$$

where

$$f_p(V,T) = \frac{\sigma^0_{p,obs}(V,T)}{\sigma^0_{p,sim}(V,T)} \tag{5}$$

Since the absolute variations of σ^0 as given by $f_p(V,T)$ may be shifted due to statistical wind speed biases and may have different scaling at various wind speeds because T_{GMF} varies with V for NSCAT-4, $f_p(V,T)$ is further normalized by its value at certain reference SST T_0, e.g., T_0=12.5°C, such that,

$$g_p(V,T) = \frac{f_p(V,T)}{f_p(V,T_0)} \tag{6}$$

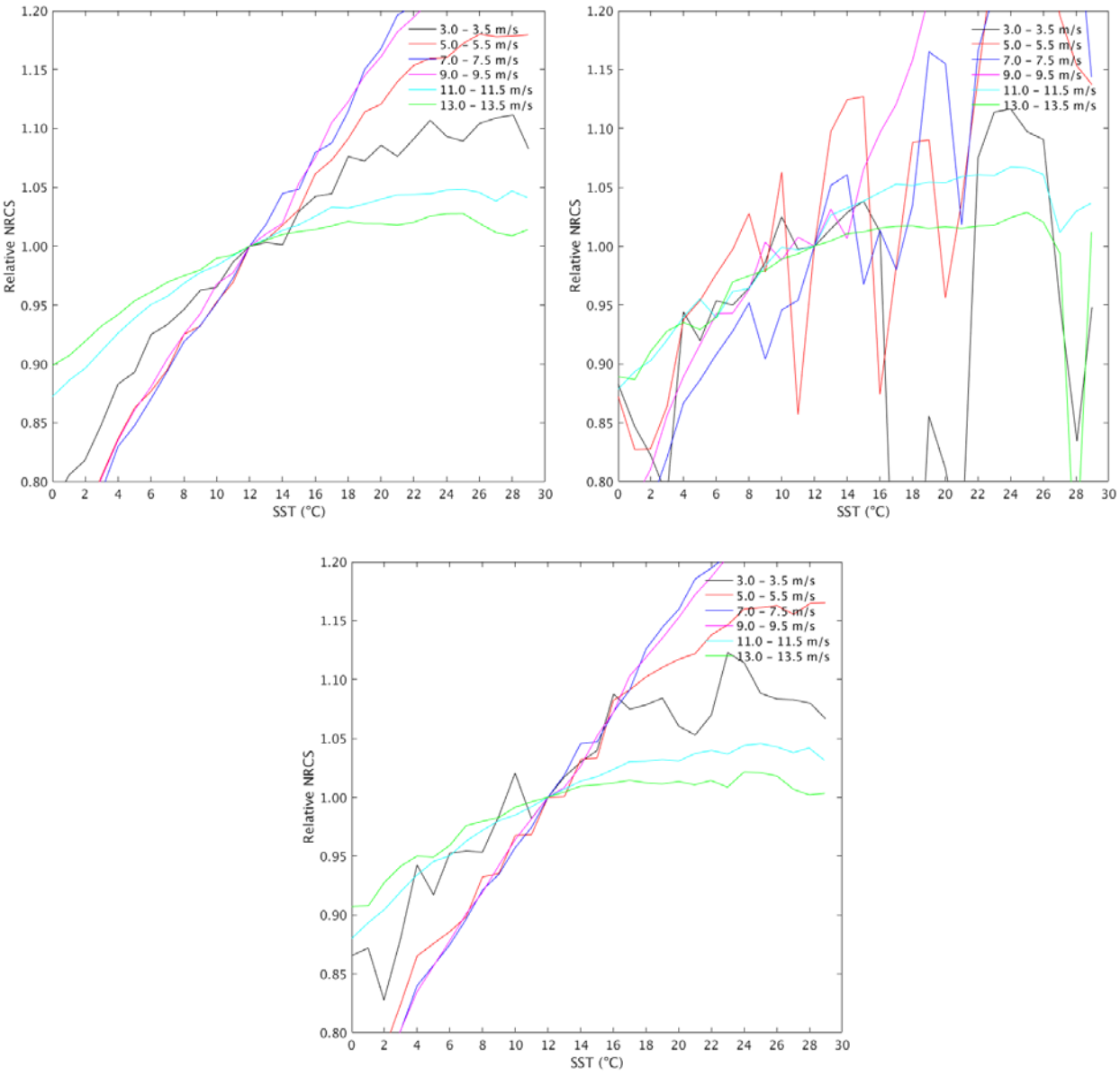

Fig. 6 g_{VV} as a function of SST, for several wind speed bins (see colour legend), and for different QC algorithms: REF-QC (a), KNMI-QC (b), and RIGO-QC (c).

Figure 6 shows g_{VV} as a function of SST, for several wind speed bins, and for the three different QC algorithms: REF-QC, KNMI-QC and RIGO-QC. Again, the KNMI-QC, which is the least conservative QC, shows a very noisy pattern, which makes it very difficult to determine the actual g_{VV} sensitivities. RIGO-QC, which shows a similar rejection pattern as that of the KNMI-QC (Fig. 5b) but with a rejection rate 3-4 times larger, shows very similar g_{VV} sensitivities to SST as those of the REF-QC (see Figs. 6a and 6c). The same results are found for g_{HH}, f_{VV}, and f_{HH} (not shown). This again indicates that as long as the most variable σ^0 measurements (e.g., due to increased wind

variability and/or residual rain contamination) are filtered out, the main σ^0 sensitivities of the GMF become rather regular and do not depend on QC. Note also that the σ^0 sensitivities for high winds (see, e.g., g_{VV} green and cyan lines in Fig. 6) are very similar for all three QC schemes, indicating that all three QCs are effective in filtering increased variability conditions at high winds.

4 SCATSat-1 QC

Generally, the scatterometer-derived winds are of high quality, and widely used in applications such as nowcasting, short-range forecasting, and numerical weather prediction (NWP) data assimilation among others. However, several geophysical phenomena other than wind, such as rain, wind variability, confused sea state, and land/ice/ship contamination within the radar footprint, can also contribute to the radar backscatter, hence distort the area mean wind-induced σ^0 measurements and degrade the retrieved wind quality [15][22]. Note that the presence of rain is a particularly acute problem for Ku-band scatterometer systems [16], such as SCATSat-1. A quality control is required to discern between good- and poor-quality winds, such that the latter can be filtered out.

Critical in QC are the False Alarm Rate (FAR), which must be minimized, and the Probability of Detection (PoD), which should be maximized. We've seen in the previous section that for quantifying SST dependencies, a critical QC with very high PoD is optimal, taking for granted a high FAR too. In many other application, these FAR points are in fact very informative as they tend to report reliable winds, but in rather variable and thus dynamic and very relevant weather conditions. A PoD above 50% and a FAR below 50% appears a reasonable compromise for QC in the presence of rain.

The proposed QC method is based on two-quality sensitive parameters, i.e., the inversion residual or MLE and the singularity exponent (SE) based on singularity analysis (SA). The MLE, a commonly used QC indicator, depicts the minimum distance between the backscatter measurements and the scatterometer GMF. A large MLE value corresponds to a large inconsistency between the σ^0 measurements and the GMF, indicating that geophysical conditions other than WVC-mean wind dominate the backscatter signal [15] [23]. For both C-band [1] and Ku-band [16] scatterometers, the SA image processing technique, has proven to be complementary to MLE. In this section, the QC approach developed for the RapidSCAT Ku-band scatterometer [16] is adapted here for SCATSat-1 QC purposes. In [16], besides the MLE and the SA-derived SE, the mean MLE or MLE_m, which is simply calculated by averaging the MLE values within a centered 3×3 box is used to improve the effectiveness of QC. Note that, as mentioned in section 2, the SCATSat-1 winds used in this section are processed with the new NSCAT-5 GMF [18], which consists of NSCAT-4 with direction and speed corrections, and the consolidated SST σ^0 corrections tailored for ScatSat-1 incidence angles.

4.1 Characterization of QC indicators

In this section, the sensitivity of the different SCATSat-1 derived quality-sensitive parameters, i.e., MLE, MLE_m and SE, to wind quality is assessed using the collocated ASCAT wind data and the Global Precipitation Measurement (GPM) satellite's Microwave Imager (GMI) rain data. The collo-

cated data are separated into inner- (VV + HH) and outer- (only VV) swath WVCs, and into 21 speed bins of 1 m/s (the last bin includes all winds > 20 m/s) for each swath category. The inner swath data are further separated into the sweet (WVC 10-28 and 49-67) and the nadir swath (WVC 29-48) regions in order to check the impact of azimuth diversity (note that in the nadir swath, there is poor azimuth diversity, i.e., the azimuth angle separation between the different beams is either too small or too close to 180°) on the sensitivity of the proposed indicators to wind quality.

Assuming that the wind quality or the rain impact is a monotonic function of each quality indicator, the collocated data are then sorted by MLE and MLE_m in descending order, and by SE in ascending order for each of the above mentioned categories/bins. Then each set of sorted data are segregated into a series of 1% bins in order to compare the sensitivity of these indicators to wind quality or rain in a straightforward way (regardless of their actual values).

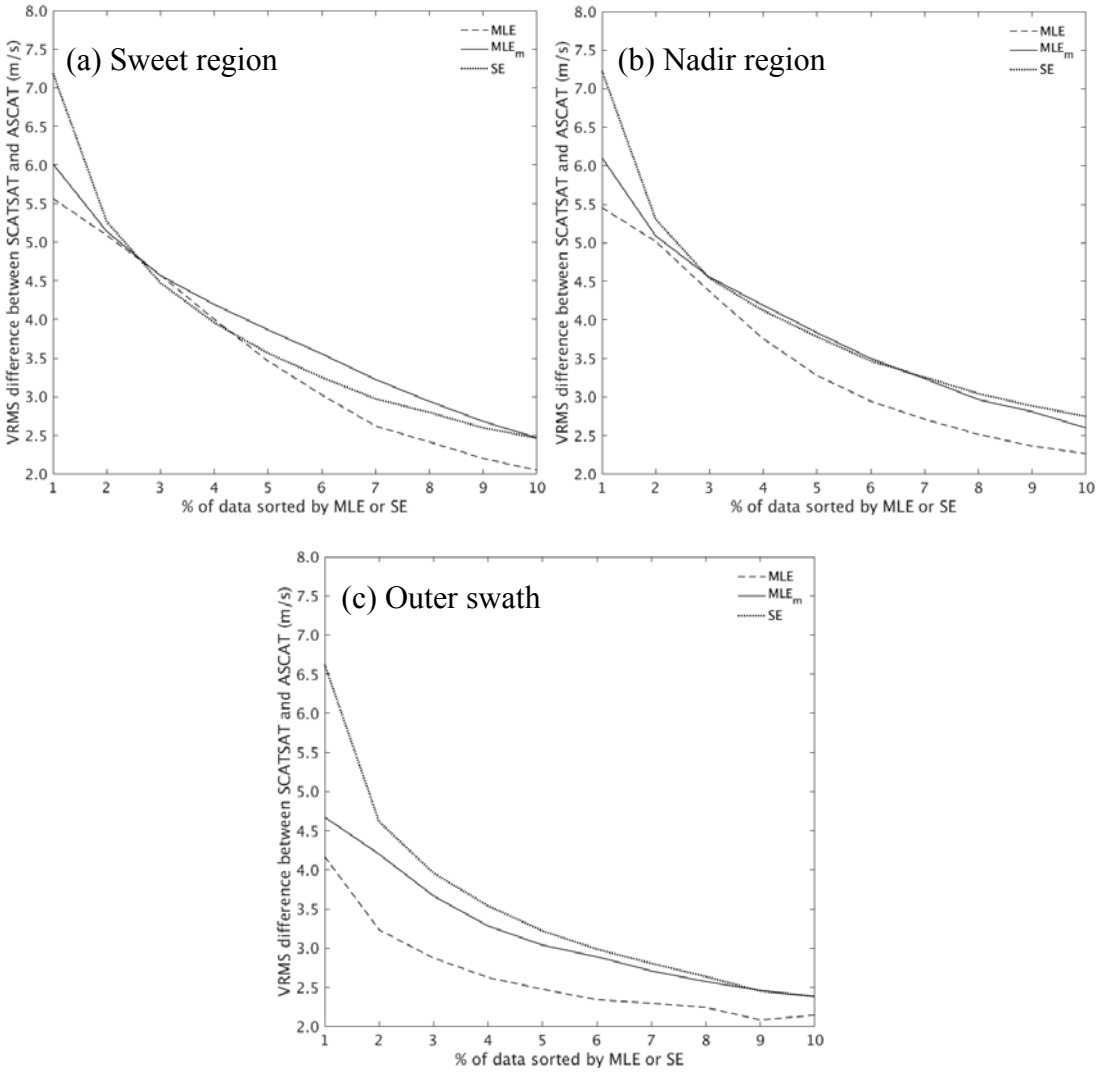

Fig. 7 VRMS difference between SCATSat-1 and ASCAT wind as a function of the sorted percentiles by MLE, MLE_m, and SE in the (a) sweet, (b) nadir, and (c) outer swath regions.

Figure 7 shows the Vector Root-Mean-Square (VRMS) difference between SCATSat-1 and ASCAT winds as a function of the percentiles sorted by MLE (dashed curve), MLE_m (solid curve)

and SE (dotted line). The same percentage of data in each speed category is used to construct the general trends of wind quality. In terms of flagging the most discrepant SCATSat-1 and ASCAT winds, the azimuth diversity does impact the sensitivity of the three indicators. In the outer swath, the lack of HH-polarized measurements is aggravated by the poor azimuth diversity of the outermost WVCs (similar to that of the nadir swath). This in turn degrades the sensitivity of each indicator to wind quality. For the inner swath region (both the sweet and the nadir regions), SE is slightly more sensitive than MLE_m and MLE, particularly for the top 2-3% of data. Furthermore, SE is clearly the most sensitive parameter to wind quality in the outer swath. MLE_m and SE have similar sensitivity to the data quality, and therefore prove to be remarkably more effective in terms of data quality classification.

Figure 8 shows the percentage of rain-contaminated data [i.e., with collocated GMI rain rate (RR) above 1 mm/h] as a function of SCATSat-1 wind speed and the sorted percentiles by MLE (left), MLE_m (middle), and SE (right), for the sweet (top row), nadir (middle row), and outer (bottom row) swath regions. The operational MLE threshold (KNMI-QC) is converted into the rejection ratio, and plotted as the white dashed curve for reference.

For MLE, in the inner swath (top left and middle left), the colour is either red or blue, which indicates that the MLE-based QC is very effective in detecting rain with high PoD (red) and low FAR (blue). The white dashed curve should ideally run at the blue-red border, e.g., at p=50%. However, while it indeed excludes a high ratio of rainy data to its left in the top left panel, it crosses a GMI RR percentile of only 10%. Flagging rain when 90% of the points has no rain will not be optimal for most applications (FAR=90%, PoD=10%), which suggests that the sweet swath QC could be made stricter, based on the MLE. We note that such stricter QC would affect the results in the remainder of this report. MLE_m (see top-middle and middle-middle) has more rain bins with PoD>50%, which implies that a larger percentage of data (more percentiles) need to be flagged to remove rain with some certainty (50%). This is consistent with the presence of more intermediate colours (slightly more dispersion) than for MLE and thus MLEm appears slightly less effective than MLE for rain flagging (also see, for the top and middle rows, the larger accumulation of blue-ish bins at the left side of the white line in the left column plots as compared to those in the middle columns). On the other hand, for winds above 15 m/s, MLE_m can be used to identify more certain rain-free data (PoD<10%) than MLE (see, for the top and middle rows, the larger blue-coloured area in the middle column plots than those in the left and right columns) at high winds conditions. We note that rain contamination generally leads to Ku-band scatterometer retrieved winds around 15 m/s. Such wind regime is therefore of particular interest for Ku-band QC purposes. In general, in the inner swath (i.e., both the sweet and the nadir regions), MLE_m and MLE are generally effective for rain detection purposes, while SE is not very effective. On the other hand, as shown in Figure 7, SE is comparable to MLE_m in filtering the most discrepant SCATSat-1 and ASCAT winds. This indicates that other geophysical phenomena besides rain contamination, e.g., increased local wind variability (note that rain induces increased wind variability well beyond the rainy cells [1]), also degrade the SCATSat-1 wind comparison to ASCAT, as identified by SE. This may be due to increased (ASCAT-SCATSat) collocation errors in areas with large spatial gradients (and therefore not strictly related to a quality degradation of SCATSat-1 winds) or due to a SCATSat-1 misrepresentation of the high wind variability conditions (therefore related to a quality degradation of SCATSat-1 winds). Such phenomena are more evident in the SE field than in the MLE/MLE_m fields and need further investigation, since they are of dynamical interest.

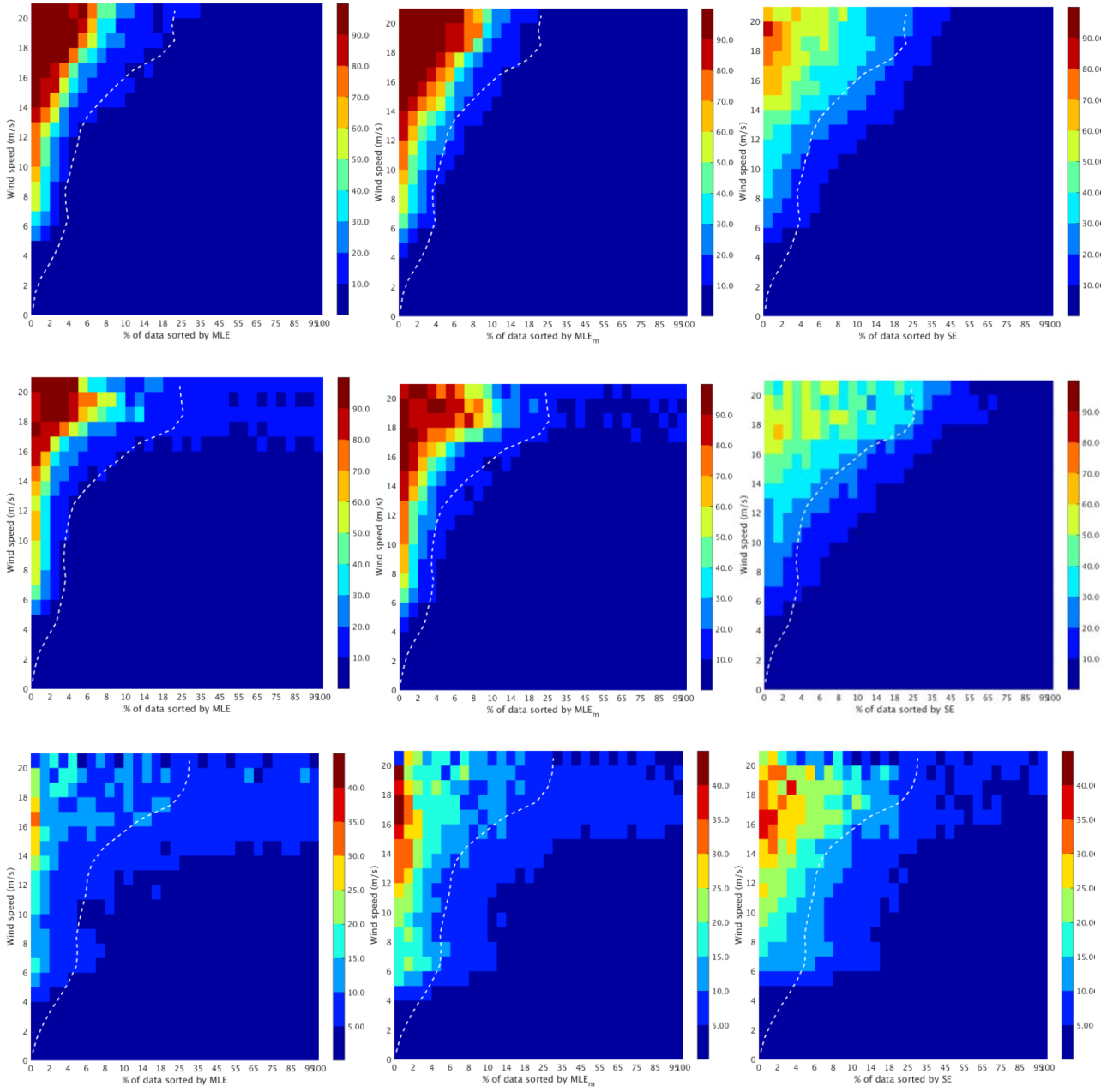

Fig. 8 Percentage p of rain-contaminated data (GMI RR > 1 mm/h, see colour legend) as a function SCATSat-1 wind speed and the sorted percentiles by (left) MLE, (middle) MLE_m, and (right) SE. The top row shows the results of the sweet-region WVCs, the middle row shows those of the nadir-region WVCs, and the bottom row shows those of the outer-swath WVCs. The white dashed curve indicates the rejection ratio of the KNMI-QC.

Note that since the ratio of rainy data (GMI RR > 1 mm/h) is about 2.5% for both the inner and the outer swath plots, it is inferred that the rain detectability is higher in the inner swath than in the outer swath (note the change of colour scale in the bottom row), while the skill for MLE and MLE_m is most degraded (see, in the left and middle columns, the higher density of rainy data in the left part of the plots for the top and middle rows as compared to the bottom row). While the rain detectability of SE (right column) is also smaller in the outer swath, in general SE skill is now comparable

to MLE_m and much better than MLE skill.. In the outer swath, the lack of HH-polarized beams and the poor azimuth diversity of the outermost WVCs leads to an inversion residual (MLE) that is noisy and therefore less effective as QC indicator [2]. Therefore, here, SE is a complementary indicator to MLE/MLE_m in classifying Ku-band wind data quality, in particular for rain contamination in the outer swath at high winds (> 15 m/s).

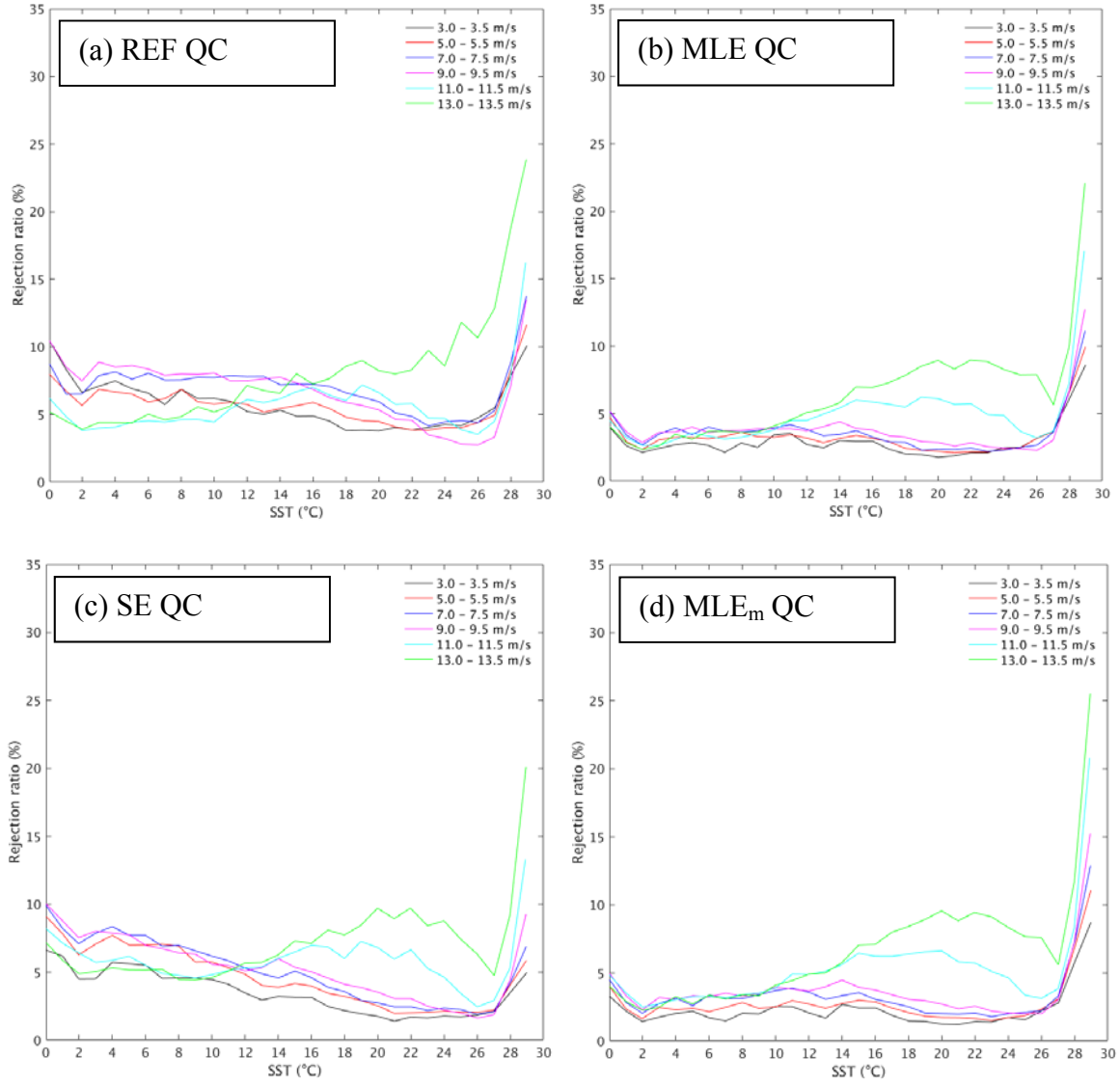

Fig. 9 Rejection ratio as a function of SST for different SCATSat-1 wind speed (after applying SST-dependent corrections) intervals (see colour legend), and for the REF-QC (a), the KNMI-QC (b), the SE-QC (c), and the MLE_m-QC (d) datasets. Only the inner swath data are used.

The top plots of Figure 9 show the same as Figure 5 but for the new SCATSat-1 reprocessed dataset using NSCAT-5. Note that as in Figure 5, the KNMI-QC leads to a rather uniform rejection ratio across SST and wind speeds, except for high winds, where rain and wind appear more confused, as expected. The REF-QC rejection ratio is now generally much smaller and less dependent on SST and wind speed than that of Figure 5, suggesting more consistent wind retrievals with smaller resid-

uals. The second row of Figure 9 shows the same as the first row but for the new MLE_m and SE QC indicators. The MLE_m-QC rejection ratio (bottom right) has a similar behaviour than that of the MLE-QC (top right), while the SE-QC rejection ratio (bottom left) behaves similarly to that of the REF-QC (top left). In general, all four QC indicators show a much smaller dependency on SST and wind speed than the REF-QC of the old SCATSat-1 dataset (Figure 5), showing that the reprocessed SCATSat-1 dataset (using NSCAT-5) is effectively mitigating such dependencies. We note that the high rejection rates at high SST (>28 ^oC) need further investigation, particularly at the higher winds.

In summary, SE is generally more effective than MLE_m and MLE in flagging the most discrepant SCATSat-1 and ASCAT winds, notably in the outer swath, which may be explained by an enhanced collocation error or actual wind quality degradation in the spatially variable conditions identified by SE. MLE/MLE_m and SE/MLE_m are the best indicators for rain in the inner and outer swath, respectively. For Ku-band scatterometer rain detection, one may use MLE and/or MLE_m over the inner-swath WVCs and SE and/or MLE_m over the outer-swath WVCs. This is further discussed in the next section.

4.2 QC verification

The objective of scatterometer QC is to maximize poor-quality rejections (including rain; PoD) while minimizing good-quality rejections (FAR). In other words, given a certain filtering objective (i.e., rejection ratio), the scatterometer QC aims to maximize the error scores (e.g., the VRMS difference between SCATSat-1 and ASCAT winds, using the latter as reference) of the rejected category, and to minimize the error scores of the preserved or accepted category. In this study, the rejection ratio of the MLE-based operational PenWP QC (KNMI-QC) is used as reference for improving the SCATSat-1 QC. The QC thresholds for MLE_m and SE are adjusted separately in the global SCATSat-1 dataset, such that the overall percentage of QC-rejected data by MLE_m and SE is equivalent to that of the KNMI-QC in each WVC and wind speed bin, though perhaps not optimal (see Figure 8). The objective then becomes to get higher VRMS scores than those of the KNMI-QC rejected category with the new methodology. Note that this is not the optimal way to determine the QC thresholds, but a straightforward method to assess the performance of different QC indicators. Finally, the three QC methods are verified using the collocated GMI and ASCAT.

Note also that since the QC thresholds for MLE_m and SE are adjusted separately in the global dataset, the percentage of QC-rejected data by MLE_m and SE can slightly differ from that of the KNMI-QC (MLE) in the collocated datasets, i.e., the SCATSat-1/ASCAT and the SCATSat-1/GMI. As shown in Figure 10, this is because of two reasons: on the one hand, as shown in Figure 10a, the global SCATSat-1 wind distribution as a function of latitude (blue curve) differs from those of the SCATSat-1/ASCAT (red curve) and SCATSat-1/GMI (magenta curve) datasets; on the other hand, the three QC indicators show a different QC-rejection ratio as a function of latitude (see Figure 10b), though quite consistent with [25]. SE rejects less (more) data than MLE/MLE_m over the tropics (extra-tropics). As such, in the collocated SCATSat-1/GMI dataset, SE-QC rejects more data (5.0%) than MLE-QC (4.6%) and MLE_m-QC (4.3%) (not shown) because of the larger accumulation of this dataset in the extra-tropics (see Figure 10a). The same happens in the SCATSat-1/ASCAT dataset although to a lesser extent since this dataset has a similar distribution to that of the global SCATSat-1 dataset (see the slightly different rejection ratios for the three QC indicators in Table 2).

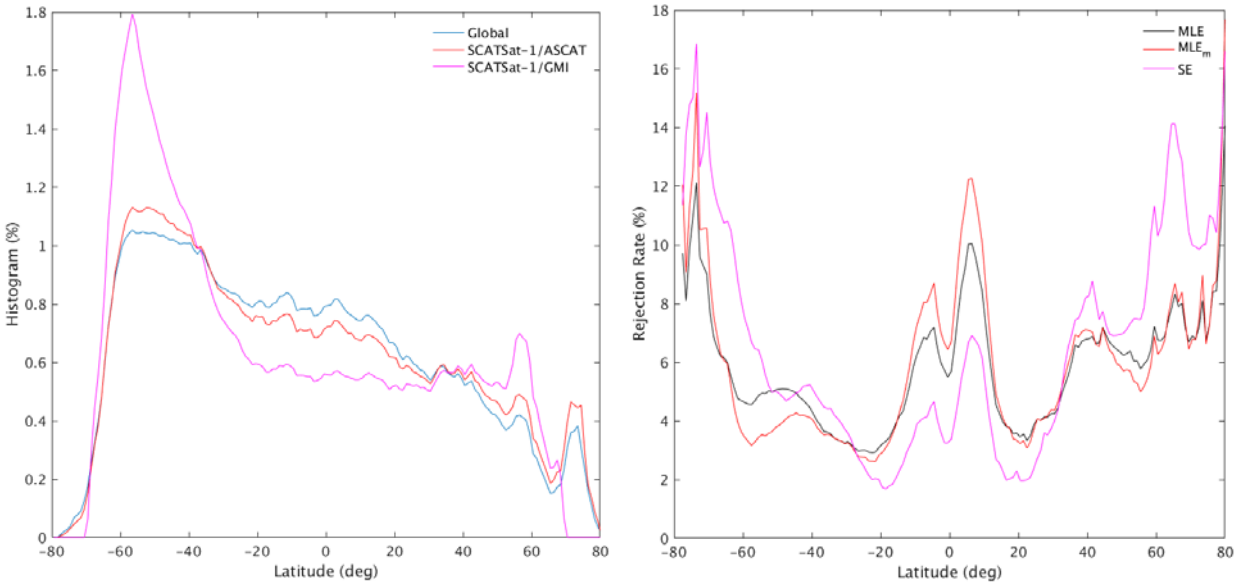

Fig. 10 (a) Normalized histogram as a function of latitude for the global SCATSat-1, the collocated SCATSat-1/ASCAT, and the collocated SCATSat-1/GMI datasets. (b) The rejection ratio as a function of latitude for the MLE, MLE_m and SE (see colour legend).

Table 1 compares the general performance of the three QC indicators in terms of rain detection. In the inner swath, MLE_m is the most effective rain indicator, due to the rather wide extension of the white line in Figure 8, followed by MLE and SE. While in the outer swath, MLE_m and notably SE outperform MLE.

Table 1. Percentage [%] of rain contaminated data over the QC-rejected data by different indicators

Swath	Percentage of GMI RR>0 mm/h			Percentage of GMI RR>1 mm/h		
	MLE	MLE_m	SE	MLE	MLE_m	SE
Sweet	52.7	63.7	47.1	28.0	34.6	24.1
Nadir	46.7	58.6	44.0	23.2	30.4	21.7
Outer	23.8	32.3	32.6	9.6	15.7	14.2

Table 2 summarizes the VRMS difference between SCATSat-1 and ASCAT winds for the accepted/rejected categories defined by MLE (KNMI-QC) and the two new QC indicators, i.e., MLE_m and SE. Generally, the SE-QC is more effective than the MLE_m-QC and the MLE-QC in filtering the most discrepant SCATSat-1 winds w.r.t. ASCAT winds, i.e., for this selected rejection ratio, the

SE-rejected winds have higher VRMS values than those of the MLE_m-rejected and MLE-rejected in every swath region. The high VRMS values for the SE-rejected wind category (see Table 2) are likely due to increased spatial wind variability at low and moderate winds. Whether this is due to degraded SCATSat-1 wind quality or to much enhanced spatial collocation error near gust lines, fronts and lows, needs to be further investigated, since this is obviously of particular user interest. Note also that, as expected, the lowest VRMS scores correspond to those of the sweet swath, where there is good azimuth diversity, thus leading to higher quality SCATSat-1 winds. Moreover, the highest VRMS scores correspond to those of the nadir swath, which implies that the azimuth diversity plays a more import role than the polarization combination in the wind retrieval quality.

As already explained, the SE-QC rejected ratio is slightly higher in all three swath regions (see Table 2). In general, SE shows more effective QC scores than MLE, in line with the earlier results. However, in the inner swath, the MLE_m QC scores are close to those of the SE. As such, further work should focus on assessing the complementarity of MLE_m and SE. For ASCAT QC, it was found that MLE and SE are actually quite complementary and a combined MLE/SE QC was proposed [1]. A combined $MLE_{(m)}$/SE may lead to a more effective SCATSat-1 QC in the inner and outer swath, although in the outer swath, the MLE_m/SE-QC are clearly the most effective.

Table 2. VRMS (m/s) difference between SCATSat-1 and ASCAT winds categorized by different QC methods and swath regions. The rejection ratio is shown in parenthesis.

Swath	MLE		MLE_m		SE	
	Accept	Reject	Accept	Reject	Accept	Reject
Sweet	1.48	4.65 (5.0%)	1.44	4.87 (5.0%)	1.36	5.14 (5.3%)
Nadir	1.84	4.57 (5.6%)	1.79	4.93 (5.7%)	1.73	5.31 (5.9%)
Outer	1.68	3.26 (4.9%)	1.60	3.82 (4.9%)	1.47	4.55 (5.0%)

5 Conclusions

In this study, an extension of a recent CDOP-2 Associated Scientist study [14] is carried out. In [14], the approach used to derive the NSCAT-5 GMF for RapidScat [12] is adapted to assess the SCATSat-1 backscatter sensitivity to sea surface wind and SST, both for HH and VV polarisations. The ASCAT winds are used as reference in the analysis. Most of the results in [14] are similar to those in [12], except that: 1) the wind speed difference dependency on relative wind direction is substantially lower in [14] than in [12]; 2) unlike [12], no SST dependency in the simulated backscatter values is found in [14]. These may be attributed to the different sampling between RapidScat and SCATSat-1 scatterometer. Moreover, remaining rain contaminated data in the QC-accepted SCATScat-1 data is suggested as a potential cause of some of these differences.

In the present study, the new version of SCATSat-1 winds (v1.1.3) collocated with ASCAT, and supplemented by ECMWF stress-equivalent winds are used in the analysis. Furthermore, the dataset is extended from 2 to 10 months to improve the sampling and better assess the impact of the different QC schemes. In particular, the impact of three different QC schemes, i.e., REF-QC (86.9% of accepted data), KNMI-QC (94.6%), and RIGO-QC (75.6%), on the GMF sensitivities is tested. It is found that indeed the main σ^0 sensitivities are preserved when using different QC thresholds. Note though that for the least conservative QC (KNMI-QC), the sensitivities of the measured σ^0 (and other related parameters such as g_{VV}, g_{HH}, f_{VV}, and f_{HH}) to SST are more irregular (noisier) than for the more conservatives REF-QC and RIGO-QC. This irregularity may be caused by the fact that the KNMI-QC dataset contains more high wind variability conditions and/or presence of rain than the REF-QC and the RIGO-QC datasets, which indeed impact the observed σ^0 sensitivities.

The SCATSat-1 data are then reprocessed using the NSCAT-5 GMF in order to develop an improved QC method. Three parameters, i.e., MLE, MLE_m, and SE, are assessed in terms of their effectiveness as QC indicators, using collocated ASCAT winds and GMI rain rate data as reference. MLE and MLE_m appear the most effective in the inner swath to uniquely detect rain, according to GMI, while SE is ineffective here for rain detection. In fact, QC by MLE may be improved in the inner swath by rejecting substantially less data, though this has not been done here. SE and MLE_m are most effective for rain detection in the outer swath, but the MLEs are generally much less effective for QC here than in the inner swath. It turns out that the SE is generally more effective than the MLE_m and the MLE in flagging the most discrepant SCATSat-1 and ASCAT winds for current QC rejection rates, notably in the outer swath. Since SE seeks for spatial wind singularities, this discrepancy between ASCAT and SCATSat-1 winds may be due to a SCATSat-1 wind quality degradation or to a substantially enhanced ASCAT/SCATSat-1 collocation error near shear lines, (gust) fronts and lows. Further investigation is needed to further conclude on this since capturing these phenomena is of particular interest to most of the scatterometer data users. This investigation is also relevant in the inner swath, since SE is not as effective rain indicator as $MLE_{(m)}$ but still obtains a high QC indicator score due to other geophysical phenomena besides rain contamination, i.e., increased local wind variability. Since MLE and SE performance appear quite different in the inner and outer swath with respect to rain and VRMS scores, the complementarity of SE and $MLE_{(m)}$ should be further explored. A combined $MLE_{(m)}$/SE may lead to a more effective SCATSat-1 QC in the inner and outer swath.

Acknowledgments

The work has been funded under the EUMETSAT Ocean and Sea Ice (OSI) Satellite Application Facility (SAF) Associated Scientist project (reference OSI_AVS_17_04). We acknowledge ISRO for putting the SCATSat-1 data available. The ASCAT and SCATSat-1 scatterometer winds are provided by EUMETSAT. The software used in this work has been developed through the EUMETSAT Numerical Weather Prediction SAF. The ECMWF data are retrieved from the ECMWF MARS archive.

Acronyms and abbreviations

Table 3 – List of acronyms and abbreviations

Name	Description
ASCAT	Advanced scatterometer
AWDP	ASCAT Wind Data Processor
BUFR	Binary Universal Form for Representation (of meteorological data)
CMOD	C-band geophysical model function used for ERS and ASCAT
CSIC	Consejo Superior de Investigaciones Científicas
ECMWF	European Centre for Medium-Range Weather Forecasts
ERS	European Remote sensing Satellite
ESA	European Space Agency
EUMETSAT	European Organization for the Exploitation of Meteorological Satellites
FAR	False Alarm Rate
GMF	Geophysical Model Function
KNMI	Koninklijk Nederlands Meteorologisch Instituut (Royal Netherlands Meteorological Institute)
METOP	Meteorological Operational satellite
MLE	Maximum likelihood estimator
NWP	Numerical Weather Prediction
OSI	Ocean and Sea Ice
PoD	Probability of Dectection
QC	Quality Control
RR	Rain rate
SA	Singularity Analysis
SAF	Satellite Application Facility
SD	Standard Deviation
SE	Singularity Exponent
WVC	Wind Vector Cell

References

[1] Wang, Z., Stoffelen, A., Fois, F., Verhoef, A., Zhao, C., Lin, M., and Chen, G., "SST dependence of Ku- and C-band backscatter measurements," *IEEE J. Sel. Top. Appl. Earth Obs. Remote Sens.*, Vol. 10, no.5, pp. xx1-12, 2017.

[2] Kloe, Jos de, Ad Stoffelen, and Anton Verhoef, Improved Use of Scatterometer Measurements by Using Stress-Equivalent Reference Winds, *IEEE J. Sel. Top. Appl. Earth Obs. Remote Sens.,* 10, (5), 2017, DOI: 10.1109/JSTARS.2017.2685242.

[3] Portabella, M., and Stoffelen, A., "Rain detection and quality control of SeaWinds," *J. Atm. and Ocean Techn.*, 18 (7), pp. 1171-1183, 2001.

[4] Lin, W., Portabella, M., Stoffelen, A., Verhoef, A., and Turiel, A., "ASCAT wind quality control near rain," *IEEE Trans. Geosci. Rem. Sens.*, 53 (8), pp. 4165-4177, 2015.

[5] Hersbach, H., Stoffelen, A., and De Haan, S., "An improved C-band scatterometer ocean geophysical model function: CMOD5", *J. Geophys. Res. Oceans*, 112(C3), 2007.

[6] Ricciadulli, L., "ASCAT on MetOp-A data product update notes", *RSS Tech. Report 040416*, Remote Sensing System, 2016.

[7] Stoffelen, A., Verspeek, J., Vogelzang, J., and Verhoef, A., "The CMOD7 Geophysical Model Function for ASCAT and ERS Wind Retrievals," *IEEE J. Sel. Top. Appl. Earth Obs. Remote Sens.*, 10(5), 2123-2134, 2017.

[8] Wentz, F. J., Peteherych, S., and Thomas, L. A., "A model function for ocean radar cross sections at 14.6 GHz,", *J. Geophys. Res. Oceans*, 89(C3), 3689-3704, 1984.

[9] Wentz, F. J., and Smith, D. K., "A model function for the ocean-normalized radar cross section at 14 GHz derived from NSCAT observations," *J. Geophys. Res. Oceans*, 104, 11499-11514, 1999.

[10] OSI SAF, Algorithm Theoretical Basis Document for the OSI SAF wind products, SAF/OSI/CDOP2/KNMI/SCI/MA/197, and "NSCAT-4 Geophysical Model Function", 2014. Available at http://projects.knmi.nl/scatterometer/nscat_gmf/ .

[11] Gohil, B. S., Sikhakolli, R., and Gangwar, R. K., "Development of geophysical model functions for Oceansat-2 scatterometer," IEEE Geoscience and Remote Sensing Letters, 10(2), 377-380, 2014.

[12] Ricciardulli, L., and Wentz, F. J., "A scatterometer geophysical model function for climate quality winds: QuikSCAT Ku-2011," *Journal of Atmospheric and Oceanic Technology*, 32(10), 1829-1846, 2015.

[13] Wang, Z., Stoffelen, A., Zhao, C., Vogelzang, J. Verhoef, A., Verspeek, J., Lin, M., and Chen, G., "A SST-dependent Ku-band geophysical model function for RapidScat," *J. Geophys. Res. Oceans*, 122(4), 3461-3480, 2017.

[14] Lin, W., Portabella, M., Stoffelen, A., Verhoef, A., and Wang, Z., "Preliminary validation of the NSCAT-5 Geophysical model function," *Associated Scientist report for the EUMETSAT OSI SAF*, SAF/OSI/CDOP3/KNMI/SCI/RP/313, available at http://www.icm.csic.es/articles, November 2017.

[15] Portabella, M., Stoffelen, A., Verhoef, A., and Verspeek, J., "A new method for improving scatterometer wind quality control," *IEEE Geosci. Rem. Sens. Lett.,* **9** (4), pp. 579-583, https://doi.org/10.1109/LGRS.2011.2175435, 2012.

[16] Lin, W., and Portabella, M., "Towards an improved wind quality control for RapidScat," *IEEE Trans. Geosci. Rem. Sens.*, **55** (7), pp. 3922-3930, https://doi.org/10.1109/TGRS.2017.2683720, 2017.

[17] Verhoef, A., Vogelzang, J., Verspeek, J., and Stoffelen, A., "PenWP user manual and reference guide," NWPSAF-KN-UD-009, Version 2.1, KNMI, De Bilt, the Netherlands, Feb. 2017.

[18] Wang, Z., Stoffelen, A., He, Y., Zhang, B., Verhoef, A., Lin, W., Li, X., and Shao, F., "An improved wind direction modulation for Ku-band geophysical model functions, based on ASCAT and OSCAT-2 collocations", *IEEE Journal of Selection Topics in Applied Earth observations and Remote Sensing*, in review, 2018.

[19] Hersbach, H., "CMOD5.n: A C-band geophysical model function for equivalent neutral wind," ECMWF technical memorandum. [Online]. Available: http://www.ecmwf.int/sites/default/files/elibrary/2008/9873-cmod5n-c-band-geophysical-model-function-equivalent-neutral-wind.pdf.

[20] Verhoef, A., Portabella, M., and Stoffelen, A., "CMOD5.n – The CMOD5 GMF for neutral winds," SAF/OSI/CDOP/KNMI/TEC/TN/165. [online]. Available: http://projects.knmi/nl/publications/fulltexts/cmod5_neutral_winds_1.0.pdf

[21] Ricciardulli, L., and Wentz, F., "Towards a climate data record of ocean vector winds: The new RSS ASCAT," in *Proc. Int. Ocean Vector Wind Sci. Team Meet.*, Kona, HI, USA, May 2013. [Online]. Available: http://coaps.fsu.edu/scatterometry/meeting/docs/2013/New_Products/Ricciardulli_ovwst_2013_ascat_winds_updated.pdf.

[22] M. Portabella, A. Stoffelen, W. Lin, A. Turiel, A. Verhoef, J. Verspeek, and J. Ballabrera-Poy, "Rain effects on ASCAT wind retrieval: Towards an improved quality control," *IEEE Trans. Geosci. Remote. Sens.*, vol. 50, no. 7, pp. 2495–2506, Jul. 2012.

[23] A. Stoffelen and D. Anderson, "Scatterometer data interpretation: measurement space and inversion," *J. Atm. and Ocean Techn.*, Vol. 14, no. 6, pp. 1298-1313, Dec. 1997.

[24] M. Portabella, A. Stoffelen, "On Scatterometer Ocean Stress", *J. Atm. and Ocean Techn.*, 26(2):368-382, DOI: 10.1175/2008JTECHO578.1

[25] Ellis, T. D., T. L'Ecuyer, J. M. Haynes, and G. L. Stephens (2009), How often does it rain over the global oceans? The perspective from CloudSat, Geophys. Res. Lett., 36, L03815, doi:10.1029/2008GL036728.